cation as a template by examining the interior volume defined by the channel and pocket features of the ZSM-18 structure. A slice of the unit cell between $z = 0$ and $z = 1/2$ can be viewed along the c axis to outline the largest interior volume projection. Since the structure of the triquat cation is known (*2, 3*), it can be drawn to scale within that volume. A stereo drawing of the triquat cation and the proposed locations of the triply charged ions within the ZSM-18 structure are shown in Fig. 4. The scaled projection drawing shows that the triquat moiety must occupy rather specific positions within the framework structure of ZSM-18. The probable arrangements of aluminosilicate anions and organic cations that would favor cocrystallization make it less surprising that a 3-ring of aluminosilicate material could form to balance the positively charged triquat. Clearly, this suggests, however, that the formation of ZSM-18 and perhaps any 3-ring aluminosilicate zeolite may depend on the judicious choice of a bulky, multiply charged, cationic templating species.

REFERENCES AND NOTES

1. J. Ciric, U.S. Patent 3,950,496 (1976).
2. ———, S. L. Lawton, G. T. Kokotailo, G. W. Griffin, *J. Am. Chem. Soc.* **100**, 2173 (1978).
3. S. L. Lawton, J. Ciric, G. T. Kokotailo, *Acta Crystallogr. Sect. C* **41**, 1683 (1985).
4. J. M. Bennett and B. K. Marcus, in *Innovation in Zeolite Materials Science*, P. J. Grobet, W. J. Mortier, E. F. Vansant, G. Schulz-Ekloff, Eds. (Elsevier, Amsterdam, 1988), vol. 37, pp. 269–279. MAPSO-46 is an aluminophosphate with the composition $Mg_6Al_{22}P_{36}Si_2O_{112}$ (Mg is an extra framework cation, and the locations of the Si impurity atoms are unknown).
5. The International Zeolite Association designation for secondary building units (SBU) for these structures requires the introduction of a new SBU, the single 3-ring, in order to describe them. For models A and B, the SBU requirements are a single 3-ring + 6≡1, where the symbol 6≡1 refers to a capped 6-ring.
6. C. Baerlocher, A. Hepp, W. M. Meier, Program DLS-76 (Eidgenössische Technische Hochschule, Zurich, revised March 1978; in-house modifications, November 1981).
7. The weighted agreement values R and σ are computed as follows (*6*):

$$R_w = \left\{ \sum_{(m,n)} \sum_j [w_j(D_j^\circ - D_j^{m,n})]^2 / \sum_j (w_j D_j^\circ)^2 \right\}^{1/2}$$

$$\sigma = \left\{ \sum_{(m,n)} \sum_j [w_j(D_j^\circ - D_j^{m,n})]^2 / (M - NV) \right\}^{1/2}$$

where w_j are the weights associated with each interatomic distance type j between atoms m and n ($D_j^{m,n}$) (such as T–O, T–T, and O–O), M is the number of distances, and NV is the number of variables. D_j° are the prescribed distances for each type and are determined by:

$$D^\circ = A + B(\mathrm{TOT} - \omega) + C(\mathrm{TOT} - \omega)^2 + \ldots,$$

where A, B, and C are constants, TOT is the calculated angle about each O, and ω is the standard T–O–T angle, for example, 145°. In our calculations, $A = 1.61$, $B = -4 \times 10^{-4}$, and $C = 0$.
8. D. K. Smith, M. C. Nichols, M. E. Zolensky, Program POWD10 (College of Earth and Mineral Sciences, Pennsylvania State University, University Park, PA, March 1983).
9. Synchrotron XRD powder data of the hydrated, uncalcined form of ZSM-18 have also been obtained; refinement of the framework and cation with the use of the Rietveld procedure is in progress.
10. W. M. Meier and D. H. Olson, *Atlas of Zeolite Structure Types* (Butterworths, London, ed. 2, 1987).
11. A. W. Chester, P. Chu, W. J. Rohrbaugh, paper presented at the North American Catalysis Society meeting, San Diego, CA, May 1987.
12. D. W. Breck, *Zeolite Molecular Sieves* (Wiley, New York, 1974), p. 636.
13. G. O. Brunner and W. M. Meier, *Nature* **387**, 146 (1989).
14. Dedicated to Julius Ciric, deceased.

16 October 1989; accepted 18 January 1990

Amazon Deforestation and Climate Change

J. SHUKLA, C. NOBRE,* P. SELLERS

A coupled numerical model of the global atmosphere and biosphere has been used to assess the effects of Amazon deforestation on the regional and global climate. When the tropical forests in the model were replaced by degraded grass (pasture), there was a significant increase in surface temperature and a decrease in evapotranspiration and precipitation over Amazonia. In the simulation, the length of the dry season also increased; such an increase could make reestablishment of the tropical forests after massive deforestation particularly difficult.

THE DISTRIBUTION OF GLOBAL VEGETATION was traditionally thought to be determined by local climate factors, especially precipitation and radiation. This view has been modified because controlled numerical experiments with complex models of the atmosphere showed that the presence or absence of vegetation can influence the regional climate (*1–3*). One implication of these results is that the current climate and vegetation may coexist in a dynamic equilibrium that could be altered by large perturbations in either of the two components. The high rate of deforestation in the Brazilian portion of Amazonia, from 25,000 to 50,000 km^2 per year (*4–7*), might thus be expected to have an effect on the regional climate. If deforestation were to continue at this rate, most of the Amazonian tropical forests would disappear in 50 to 100 years.

Removal of the Amazonian forest would also have tremendous effects on species diversity and atmospheric chemistry (*8*). The Amazon basin is host to roughly half of the world's species, and the intensity and complexity of plant-animal interactions (*9*) and the rapid nutrient cycling in the soils (*10*) make the region vulnerable to external disturbances. The Amazon is also an important natural sink for ozone and plays an important role in global tropospheric chemistry. The present study is mainly confined to the assessment of the effects of deforestation on the physical climate system.

Center for Ocean-Land-Atmosphere Interactions, Department of Meteorology, University of Maryland, College Park, MD 20742.

*Permanent affiliation: Instituto de Pesquisas Espaciais, 12201 Sao Jose dos Campos, SP, Brazil.

Quantitatively estimating the effects that large changes in terrestrial ecosystems can have on temperature, circulation, and rainfall has been difficult because the equilibrium climate is determined by complex interactions among the dynamical processes in the atmosphere and thermodynamic processes at the earth-atmosphere interface. Realistic models of the biosphere that can be coupled with realistic models of the global atmosphere have only recently been developed (*11, 12*). In this report, we describe the use of a coupled atmosphere-biosphere model (*13, 14*) to investigate the consequences of the removal of Amazon forests on climate.

In the simulations, we assumed that the

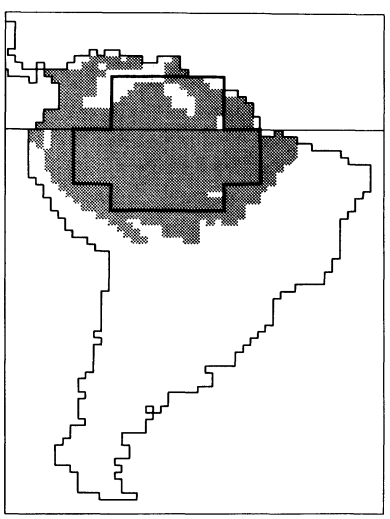

Fig. 1. The South American region. Stippling depicts the area covered by the tropical forest in the control simulation. The area marked with bold lines was used for the areal averages of Fig. 3 and for Tables 1 and 2.

Table 1. Mean surface energy budget. The data are 12-month mean (1 January to 31 December) values. Values are in watts per square meter, except for B and a, which are nondimensional, and T_s, which is in degrees centigrade. S is insolation; a is albedo; L_n is net upward long-wave radiation; R_n is available radiative energy; E_t is transpiration plus soil evaporation; E_i is interception loss; E is evapotranspiration = $E_t + E_i$; H is sensible heating; G is ground heat flux; B is the Bowen ratio (H/E); and T_s is surface temperature.

Case	S	$(1 - a)S$	L_n	R_n	E_t	E_i	E	H	G	B	a	T_s
Control	233	204	−32	172	91	37	128	44	0	0.34	12.5	23.5
Deforestation	237	186	−40	146	64	26	90	56	0	0.62	21.6	26.0
Difference	+4	−18	−8	−26	−27	−11	−38	+12	0	−0.28	+9.1	+2.5

tropical forest cover (Fig. 1) is replaced by a degraded pasture. On the basis of observed changes in soil characteristics in deforested areas (*15, 16*), we also assumed that the soils in the deforested regions are disaggregated and that, as a result, values of the soil hydraulic conductivity and water storage capacity available for transpiration are greatly reduced in the upper part of the soil profile.

We have used a high-resolution global model of the atmospheric circulation (*13*) that describes and predicts atmospheric temperature, pressure, wind, and humidity at 18 different, unequally spaced levels between the surface and 30 km. The horizontal resolution of the model at each level is about 1.8° latitude by 2.8° longitude. The large-scale topography and sea-surface temperature (SST) are prescribed. The diurnal cycle is treated explicitly in the model, and both the convective and the large-scale saturation rainfall are calculated. For radiative calculations, zonally symmetric clouds are prescribed rather than generated by the model. The global vegetation distribution at each land grid point is defined by 1 of 12 vegetation types, and each vegetation type is defined by a set of morphological, physical, and physiological parameters (*17*). There are three soil layers in the biosphere model: a thin evaporating upper layer, the root zone, and a recharge zone.

In the biosphere model (*12, 14*), the wind speed, air temperature, incident radiative flux, and precipitation as calculated from the atmospheric model are used to predict the time rate of change of the model variables: canopy temperature; ground temperature; deep soil temperature; liquid water stored on canopy foliage and ground cover foliage; and the wetness of the surface thin layer, root zone, and recharge zone. Runoff, soil moisture, and sensible and latent heat fluxes are calculated as diagnostic outputs of the model.

We first integrated the coupled atmosphere-biosphere model for 1 year with the normal prescribed global climatological boundary conditions of vegetation distribution, in which the Amazonian region is covered with tropical forests (Fig. 1); we refer to this integration as the control case. We then repeated the integrations for 1 year in which all the previous global climatological boundary conditions remained the same except over Amazonia, where the tropical forests were replaced by a degraded pasture cover consisting mainly of grass; we refer to this integration as the deforestation case. In both the control and the deforestation cases, the global SST distributions remained inadvertently fixed for the whole integration period and corresponded to the climatological mean values for December.

The changes over Amazonia in the deforestation case, in effect, resulted in the alteration of a series of climatologically significant parameters. Relative to the tropical forest, the degraded pasture cover is calculated to have a higher albedo, lower surface roughness length, higher stomatal resistance, a shallower and sparser root system, and lower available storage capacity for soil moisture. The parameters for the control case were obtained from a literature survey and from an analysis of 2 years of in situ flux measurements (*18*), whereas the parameters for the deforestation case were extracted from reports on fieldwork carried out in deforested areas (*16, 19, 20*).

The model integrations were started from an atmospheric state on 15 December, when the initial soil moisture in the region could be assumed to be at or near saturation in both cases, and integrations were carried out for 12.5 months. The results (Fig. 2) are in terms of 12-month averages (1 January to 31 December); the first 2 weeks of model integration are ignored. The annual cycle of temperature, precipitation, and evapotranspiration are shown as monthly averages.

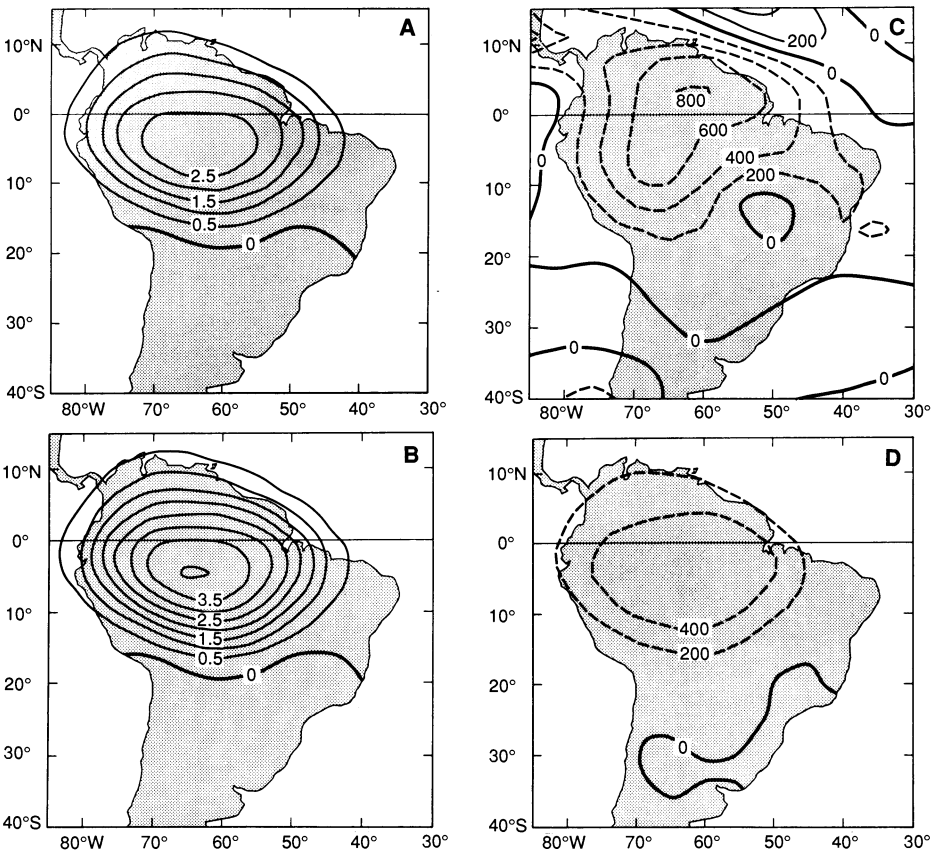

Fig. 2. Differences between 12-month means (1 January to 31 December) of deforestation and control cases (deforested − control) for the South American sector: (**A**) surface temperature increase in degrees centigrade; (**B**) deep soil temperature increase in degrees centigrade; (**C**) total precipitation changes (dashed lines indicate a decrease) in millimeters; and (**D**) evapotranspiration decrease in millimeters. Model results were smoothed before plotting.

Surface and soil temperatures are warmer by 1° to 3°C in the deforestation than in the control cases. The relative warming of the deforested land surface and the overlying air is consistent with the reduction in evapotranspiration and the lower surface roughness length. This result is in agreement with results of an earlier simulation experiment (*21*) and some observations (*22, 23*) for tropical forests.

The increase in surface temperature calculated in the deforestation case is reflected in differences in the surface energy budget for the two cases (Table 1). The absorbed solar radiation at the surface is reduced in the deforestation case (186 W/m^2) relative to the control case (204 W/m^2) because of the higher albedo (21.6%) for grassland compared to forest (12.5%). The higher surface temperature in the deforestation case gives rise to more outgoing long-wave radiation from the surface compared to the control case, so that the amount of net radiative energy available at the surface for partition into latent and sensible heat flux is considerably smaller in the deforestation case. In addition, the reduced storage capacity for soil moisture in the deforestation case has the effect of reducing the time-averaged transpiration rate; also, in the deforestation case, less precipitation is intercepted and reevaporated as the surface roughness and the canopy–water holding capacity of the pasture are relatively small.

Table 2. Mean water budget. The data are 12-month mean (1 January to 31 December) values. Values E and P are in millimeters per year; PW is in millimeters. P is total precipitation; E is evapotranspiration; and PW is precipitable water.

Case	P	E	$(E - P)$	E/P	PW
Control	2464	1657	−807	0.67	37.7
Deforestation	1821	1161	−660	0.63	35.4
Difference	−643	−496	+147	−0.04	−2.3
		Change (in percent)			
	−26.1	−30.0	+18.0	−5.9	−6.1

The reduction in calculated annual precipitation by 642 mm and in evapotranspiration by 496 mm (Table 2) suggests that changes in the atmospheric circulation may act to further reduce the convergence of moisture flux in the region, a result that could not have been anticipated without the use of a dynamical model of the atmosphere. Increased surface and soil temperatures produce some increase in the sensible heat flux (about 10 to 20 W/m^2, not shown); however, even the increased warming of the near-surface air is not sufficient to increase the convergence of air (and moisture) into the region in the simulation.

Because evapotranspiration from the forest is one of the important sources of water vapor (*24, 25*) for precipitation in the Amazon, a reduction in evapotranspiration is expected to lead to a reduction in precipitation. However, because of the complexity of the atmosphere-biosphere system and the continuous interactions of dynamical and hydrological processes, a reduction in evaporation might be compensated for by an increase in moisture flux convergence. Our experiments indicate that such a compensation will not occur for the Amazon and that there is even a further decrease in convergence of the large-scale moisture flux. Whether this result is model-dependent can only be resolved by additional experiments and comparison with results from other models.

The differences in monthly mean surface temperature, precipitation, evapotranspiration, and evapotranspiration minus precipitation for the control and the deforestation cases are consistently of the same sign but of different magnitude for each of the individual months (Fig. 3). This consistency is partly a result of the large area for spatial averaging; similar time series for different, smaller subregions of the Amazon will show more variability from one season to the other. The value of evapotranspiration minus precipitation increased in the deforestation simulation. Runoff was also reduced in the deforestation case because the decrease in precipitation was more than the decrease in evapotranspiration.

A few significant changes in global circulation were also evident in the deforestation simulation, especially over North America; however, climatic fluctuations over the northern mid-latitudes are generally large in nature as well as in simulations even without any forced perturbations, and thus the anomalies may not be directly a result of the deforestation simulation. Moreover, the artificial constraint of time-invariant SST

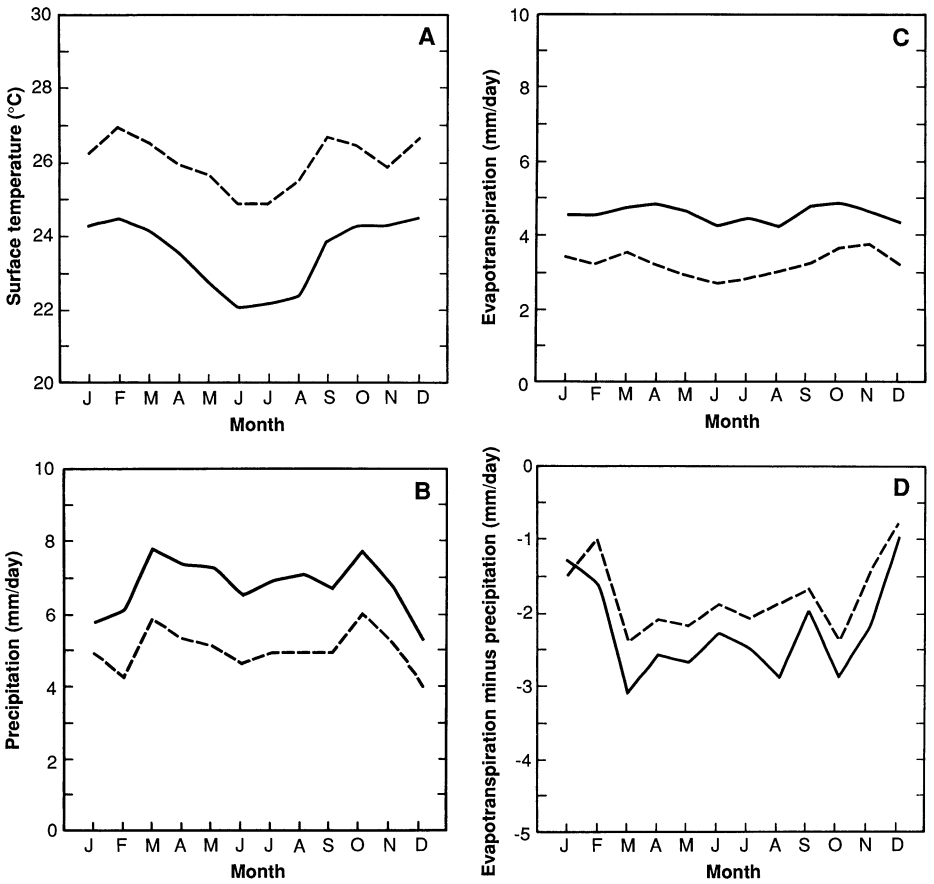

Fig. 3. Monthly distribution (1 January to 31 December) of the areal average of (**A**) surface temperature; (**B**) total precipitation; (**C**) evapotranspiration; and (**D**) evapotranspiration minus total precipitation. The solid line is for the control case, and the dashed line is for the deforestation case. Areal averages were taken over the area marked with bold lines in Fig. 1.

fields makes it difficult to draw any definitive conclusions about the global effects of Amazon deforestation from this study.

The most significant result of this study is the simulated reduction in precipitation over Amazonia, which is larger than the corresponding regional reduction in evapotranspiration, implying that the dynamical convergence of moisture flux also decreased as a result of deforestation. The spatial and temporal coherence of the decrease in precipitation implies that the deforested case is associated with a longer dry season. The lack of an extended dry season apparently sustains the current tropical forests, and therefore a lengthening of the dry season could have serious ecological implications (*26–28*). Among other effects, the frequency and intensity of forest fires could increase significantly (*29, 30*) and the life cycles of pollination vectors could be perturbed.

These results suggest that a complete and rapid destruction of the Amazon tropical forest could be irreversible. Changes in the region's hydrological cycle and the disruption of complex plant-animal relations could be so profound that, once the tropical forests were destroyed, they might not be able to reestablish themselves.

REFERENCES AND NOTES

1. J. G. Charney, W. J. Quirk, S.-H. Chow, J. Kornfield, *J. Atmos. Sci.* **34**, 1366 (1977).
2. J. Shukla and Y. Mintz, *Science* **215**, 1498 (1982).
3. Y. Mintz, in *The Global Climate*, J. T. Houghton, Ed. (Cambridge Univ. Press, Cambridge, 1984), pp. 79–106.
4. P. M. Fearnside, in *The Geophysiology of Amazonia*, R. E. Dickinson, Ed. (Wiley, New York, 1987), pp. 37–61.
5. Instituto de Pesquisas Espaciais (INPE), *Avaliação da cobertura florestal na Amazonia Legal Utilizando Sensoriamento Remoto Orbital* (INPE, Sao José dos Campos, SP, Brazil, 1989).
6. N. Meyers, *Acta Amazonica* **12**, 745 (1982).
7. D. J. Mahar, *Government Policies and Deforestation in Brazil's Amazon Region* (World Bank, Washington, DC, 1989).
8. R. A. Houghton *et al.*, *Nature* **316**, 617 (1985).
9. S. A. Mori and G. T. Prance, in *The Geophysiology of Amazonia*, R. E. Dickinson, Ed. (Wiley, New York, 1987), pp. 69–90.
10. A. C. C. P. Dias and S. Nortcliff, *Trop. Agric.* **62**, 207 (1985).
11. R. E. Dickinson, A. Henderson-Sellers, P. J. Kennedy, M. F. Wilson, *Biosphere-Atmosphere Transfer Scheme (BATS) for the NCAR Community Climate Model* (Tech. Note TN-275+STR, National Center for Atmospheric Research, Boulder, CO, 1986).
12. P. Sellers, Y. Mintz, Y. C. Sud, A. Dalcher, *J. Atmos. Sci.* **43**, 505 (1986).
13. J. L. Kinter, J. Shukla, L. Marx, E. K. Schneider, *ibid.* **45**, 2486 (1988).
14. N. Sato *et al.*, *ibid.* **46**, 2757 (1989).
15. H. Shubart, W. J. Junk, M. Petrere, Jr., *Ciencia Cult. (Sao Paulo)* **28**, 507 (1976).
16. C. Uhl *et al.*, *J. Ecol.* **76**, 663 (1988).
17. J. L. Dorman and P. J. Sellers, *J. Appl. Meteorol.* **28**, 833 (1989).
18. P. J. Sellers, W. J. Shuttleworth, J. L. Dorman, A. Dalcher, J. M. Roberts, *ibid.*, p. 727.
19. M. M. Ludlow, M. J. Fisher, J. R. Watson, *Aust. J. Plant Physiol.* **12**, 131 (1985).
20. G. T. Prance and T. E. Lovejoy, *Amazonia* (Pergamon, New York, 1984).
21. R. E. Dickinson and A. Henderson-Sellers, *Q. J. R. Meteorol. Soc.* **114**, 439 (1988).
22. B. S. Ghuman and R. Lal, in *The Geophysiology of Amazonia*, R. E. Dickinson, Ed. (Wiley, New York, 1987), pp. 225–244.
23. T. L. Lawson, R. Lal, K. Oduro-Afriyie, in *Tropical Agriculture Hydrology*, R. Lal and E. W. Russel, Eds. (Wiley, New York, 1981), pp. 141–151.
24. E. Salati and P. B. Vose, *Science* **225**, 129 (1984).
25. W. J. Shuttleworth *et al.*, *Q. J. R. Meteorol. Soc.* **110**, 1143 (1984).
26. H. N. Le Houerou and G. F. Popov, *An Eco-Climate Classification of Intertropical Africa* (Food and Agriculture Organization, Rome, 1978).
27. W. Lauer, in *Ecosystems of the World: Tropical Rain Forest Ecosystems*, M. Leith and M. J. A. Werger, Eds. (Elsevier, New York, 1989), vol. 14B, pp. 7–54.
28. A. Hamilton, *ibid.*, vol. 14B, pp. 155–182.
29. H. O'R. Sternberg, *Geogr. Ann. Ser. A* **69**, 201 (1987).
30. R. L. Sanford, Jr., J. Saldarriaga, K. E. Clark, C. Uhl, R. Herrera, *Science* **227**, 53 (1985).

31. We thank J. Kinter, L. Marx, M. Fennessy, and E. Schneider for help in conducting this simulation experiment, P. Dirmeyer for help in the processing and diagnosis of model outputs, and A. D. Nobre for providing information about the Amazonian ecosystem. We also thank S. Busching for help in the preparation of the manuscript and L. Rumburg for drafting the final figures. This research was supported by National Science Foundation grant ATM-87-13567 and National Aeronautics and Space Administration grants NAGW-1269 and NAGW-557.

13 October 1989; accepted 14 December 1989

Fossil Soils and Grasses of a Middle Miocene East African Grassland

GREGORY J. RETALLACK, D. P. DUGAS, E. A. BESTLAND

Fossil soils and grasses from the well-known Miocene mammal locality of Fort Ternan, southwestern Kenya, are evidence of a mosaic of grassy woodland and wooded grassland some 14 million years ago. This most ancient wooded grassland yet known on the African continent supported more abundant and diverse antelopes than known earlier in Africa. Ape fossils at Fort Ternan, including *Kenyapithecus wickeri*, were associated with woodland parts of the vegetation mosaic revealed by paleosols. Grassland habitats were available in East Africa long before the evolutionary divergence of apes and humans some 5 to 10 million years ago.

SAVANNA ECOSYSTEMS HAVE LONG been linked with early human evolution, and the antiquity of savannas in Africa has been a source of debate (*1*). Part of the problem is the loose use of the term "savanna" to include any kind of tropical grassland. We prefer the term "wooded grassland" for well-drained grassy vegetation with 10 to 40% cover by trees (*2*). Unlike wooded and open grassland, grassy woodland and marsh are at least as old as 23 million years and remained widespread 17 million years ago in East Africa, judging from evidence of paleosols (*3*), of fossil sedges and grasses (*4*), of fossil dicots (*5*), and of fossil birds allied to modern forms now found widely in grassy vegetation (*6*). Of more interest from the point of view of the evolution of African mammals is the origin of wooded grassland and open grassland among more ancient kinds of woodland and forest vegetation.

Paleosols can be useful in deciphering ancient vegetation mosaics, because, unlike fossils, they are by definition in the place they formed. They are also abundant and have been widely recognized in southwest Kenya (*3, 7–9*). The thin, brown, nodular, calcareous paleosols found throughout the 9.6-km outcrop of the middle Miocene Fort Ternan Beds are distinct from geologically older paleosols in Kenya (*3, 10*). The Fort Ternan beds are a sequence of carbonatite-nephelinite tuffs, lahars, colluvium, and alluvium. They have been dated by the K/Ar method at 14.4 ± 0.2 million years old by the use of biotite (*7, 11*). This account details only paleosols in the 8-m-thick sequence exposed in the large (*12*) quarry for fossils at Fort Ternan National Monument. Three distinct kinds of paleosols were recognized and named informally from the local Dholuo language: Chogo ("bone"), Onuria ("yellow"), and Dhero ("thin") paleosol series. The paleosols were characterized in the field, petrographically, and chemically (*13*). From these data (Fig. 1), some aspects of the original soils and their environment can be reconstructed.

One approach to interpreting paleosols is to identify them within a soil classification and compare them to modern soils, with allowance for possible alteration after burial. The distinctive surface horizons of both Onuria and Chogo paleosols are critical to their identification: they have the granular structure, thickness, dark color, and large proportion of bases that define a mollic epipedon and Mollisols (*14*). Organic mat-

G. J. Retallack and E. A. Bestland, Department of Geological Sciences, University of Oregon, Eugene, OR 97403.
D. P. Dugas, Department of Geography, University of Oregon, Eugene, OR 97403.